Exactly solvable coupled-channel potential models of atom-atom magnetic Feshbach resonances from supersymmetric quantum mechanics

Andrey M. Pupasov,[1] Boris F. Samsonov,[1] and Jean-Marc Sparenberg[2]
[1]*Physics Department, Tomsk State University, 36 Lenin Avenue, 634050 Tomsk, Russia*
[2]*Physique Quantique, Université Libre de Bruxelles, Code Postal 229, B 1050 Bruxelles, Belgium*
(Received 3 September 2007; revised manuscript received 15 November 2007; published 30 January 2008)

Starting from a system of N radial Schrödinger equations with a vanishing potential and finite threshold differences between the channels, a coupled $N\times N$ exactly solvable potential model is obtained with the help of a single nonconservative supersymmetric transformation. The obtained potential matrix, which subsumes a result obtained in the literature, has a compact analytical form, as does its Jost matrix. It depends on $N(N+1)/2$ unconstrained parameters and on one upper-bounded parameter, the factorization energy. A detailed study of the model is done for the 2×2 case: a geometrical analysis of the zeros of the Jost-matrix determinant shows that the model has zero, one, or two bound states, and zero or one resonance; a compact formula for the open-channel scattering length is obtained. As a first physical application, exactly solvable 2×2 atom-atom interaction potentials are constructed, for cases where a magnetic Feshbach resonance interacts with a bound or virtual state close to threshold, which results in a large background scattering length.

DOI: 10.1103/PhysRevA.77.012724 PACS number(s): 03.65.Nk, 24.10.Eq, 34.20.Cf, 34.50.−s

I. INTRODUCTION

Coupled-channel quantum-scattering models are today experiencing a strong renewal of interest, mainly thanks to the impressive experimental progress in the field of ultracold gases. Actually, an indispensable tool to control the atom-atom interactions in these systems relies on the coupling between channels defined by different hyperfine states of the atom-atom pairs. When dipped in a magnetic field, these hyperfine states have threshold energies that vary linearly with the field. At ultracold temperatures, the lowest-threshold state is the only open channel, while states with higher thresholds are closed. When the field is varied in a well-chosen range, quasibound states of the closed channels can appear as resonances in the open channel, a phenomenon known as a "Feshbach resonance" and first studied in nuclear physics [1,2]. When a Feshbach resonance crosses the open-channel threshold, due to magnetic-field variation, the scattering length a, which effectively controls the atom-atom interaction, goes through infinite values, switching from positive to negative sign [3–5]. This very spectacular phenomenon is now known as a magnetic-field-induced Feshbach resonance, or just magnetic Feshbach resonance.

The practical importance of magnetic Feshbach resonances has motivated various theoretical models, which can be classified in three categories: (i) microscopic models, which should in principle deduce magnetic-Feshbach-resonance properties from many-electron calculations; (ii) effective potential models, which reduce the complexity of the many-electron problem to a two-atom coupled-channel problem (usually two channels are enough), where the interaction between the two atoms is modeled by a symmetric (2×2 for a two-channel model) potential matrix; (iii) effective scattering-matrix models, which reduce the role of the underlying interactions to its impact on the atom-atom open-channel scattering matrix. Present-day theoretical descriptions of ultracold gases require only the knowledge of the atom-atom scattering length, which is directly related to the open-channel scattering matrix. As far as practical applications are concerned, the third category of models is thus sufficient. There, a magnetic Feshbach resonance is described as a pole of the scattering matrix in the complex wave-number planes, like any resonance [6], and the whole complexity of the many-electron or atom-atom problem is reduced to a few parameters of the scattering-matrix Padé expansion [7]. These parameters can be numerically obtained, e.g., with the help of the reaction-matrix method [8], from a given microscopic or effective-potential model.

In several contexts, the use of effective-scattering-matrix models is, however, increasingly felt to be insufficient. This is the case, for instance, when a magnetic Feshbach resonance occurs with a large background scattering length, due to a bound or virtual state in the open channel, close to its threshold [7]. Such an open-channel state is also called a "potential resonance" because it naturally occurs in a potential model, even in a single-channel case. Other situations where a more detailed knowledge of the atom-atom interaction than just the scattering length might be necessary are cases where molecules can be formed, as in crossovers between a Bardeen-Cooper-Schrieffer superfluid and a Bose-Einstein condensate, or in Bose-Einstein-condensate collapses. None of these cases probably requires solution of the full many-body electronic problem; effective-potential models, on the other hand, look like a reasonable approximation, as they allow for a realistic description of the atom-atom interaction in terms of the accessible channels and as a function of the radial coordinate r between atoms.

There is thus an interest in obtaining exactly solvable coupled-channel potential models with threshold differences. The first example coming to mind is probably the coupled square-well potential, which can display both potential and Feshbach resonances, as well as bound states [9]. This model has, however, two drawbacks: first, despite its simplicity and exactly solvable character, its scattering-matrix poles are given by rather complicated implicit equations. Second, its discontinuous form factor is rather limiting and very differ-

ent from the known long-range atom-atom polarization interaction. The next choice for realistic atom-atom interactions is thus a purely numerical resolution of the coupled-channel Schrödinger equation with smooth phenomenological potentials. This lack of exactly solvable potentials can be related to the poor knowledge of the scattering inverse problem (i.e., the construction of a potential in terms of its bound- or scattering-state physical properties) in the coupled-channel case with threshold differences [10]. In Ref. [11], however, Cox derives an exactly solvable coupled-channel potential with threshold differences, two remarkable features of which are the compact expressions provided both for the potential and for its Jost matrix. Since the Jost matrix completely defines the bound- and scattering-state properties of a potential model [12,13], such an analytical expression seems very promising in the context of the scattering inverse problem.

The work of Cox has, however, received little attention, probably because it appears to have two problems. First, the method of getting the potential is rather complicated: the paper mostly consists of a check that the provided analytical expression for the solutions satisfies the coupled-channel Schrödinger equation with the provided analytical expression for the potential. Not much information is given on how these expressions were obtained, which makes any generalization of the method difficult. The second problem, already discussed in Ref. [11], is that, despite the compact expression of the Jost matrix, calculating the corresponding bound- and resonant-state properties is a difficult task because these states correspond to zeros of the *determinant* of the Jost matrix in the intricate structure of the energy Riemann sheet, which has a multiplicity 2^N for N channels.

The first problem was solved recently, when it was realized that the Cox potential, at least in its simplest form ($q=1$ in Ref. [11]), can be obtained by a single supersymmetric transformation of the zero potential [14,15]. This leads to a much simpler derivation of this potential and naturally enables several generalizations of it; in particular, the initial potential is now arbitrary. The transformation used to get this result belongs to a category of supersymmetric transformations not much used up to now, namely, transformations that do not respect the boundary condition at the origin (the so-called *nonconservative* transformations; see, e.g., Ref. [14]): a solution of the initial potential vanishing at the origin is transformed into a solution of the transformed potential which is finite at the origin. This feature makes the transformation of the Jost matrix more complicated to calculate than for usual conservative transformations but it is also the key to getting potentials with nontrivial coupling. In Sec. II below, we give several alternative expressions for the Cox potential and explicitly make the link between the supersymmetric derivation and the expressions found in Ref. [11], for an arbitrary number of channels N. With respect to Refs. [14,15], this result is new as these references mostly concentrate on generalizations of the Cox potential allowed by supersymmetric quantum mechanics and on $N=2$ examples. We also show in Sec. II that the Cox potential contains the maximal number of arbitrary parameters allowed by a single nonconservative supersymmetric transformation, which makes it the most interesting potential from the point of view of the scattering inverse problem; we also derive a necessary and sufficient condition for the regularity of the potential.

The second problem, i.e., the calculation of bound- and scattering-state properties from the analytical Jost function, is touched upon in Sec. III. There, the discussion is limited to $N=2$ (a case complicated enough from the mathematical point of view but very rich already from the physical point of view). First, the number of bound and resonant states is studied geometrically in terms of the potential parameters, as well as the necessary and sufficient condition for a regular potential (several mistakes made in Ref. [11], in particular regarding the number of bound states, are corrected in passing). Second, the low-energy behavior of the open-channel scattering matrix is studied, with ultracold gases in mind. This discussion makes possible a first practical use of this potential as a schematic model of atom-atom magnetic Feshbach resonances, which is described in Sec. IV. There, an exactly solvable model is established in cases where a magnetic Feshbach resonance interplays with a potential resonance, which results in a large background scattering length, either positive (interplay with a bound state) or negative (interplay with a virtual state). This physical context is mostly inspired by Ref. [7]. Section V finally summarizes our findings and discusses possible extensions of them, in particular to other fields of physics where coupled-channel models are known to play an important role.

II. THE COX POTENTIAL FROM SUPERSYMMETRIC QUANTUM MECHANICS

Let us first summarize the notations used below for coupled-channel scattering theory [6,12,13]. We consider a multichannel radial Schrödinger equation that reads in reduced units

$$H\psi(k,r) = K^2\psi(k,r), \tag{1}$$

with

$$H = -\frac{d^2}{dr^2} + V, \tag{2}$$

where r is the radial coordinate, V is an $N\times N$ real symmetric matrix, and ψ may be either a vector-valued solution or a matrix-valued solution with linearly independent columns. By k we denote a point in the space $\mathbb{C}^N$, $k=\{k_1,\ldots,k_N\}$, $k_i\in\mathbb{C}$. A diagonal matrix with nonvanishing entries k_i is written as $K=\mathrm{diag}(k)=\mathrm{diag}(k_1,\ldots,k_N)$. The complex wave numbers k_i are related to the center-of-mass energy E and the channel thresholds $\Delta_1,\ldots,\Delta_N$, which are supposed to be different from each other, by

$$k_i^2 = E - \Delta_i. \tag{3}$$

For simplicity, we assume here that the different channels have equal reduced masses, a case to which the general situation can always be formally reduced [12]. We also assume potential V to be short ranged at infinity and to support a finite number M of bound states. Under such assumptions,

the Schrödinger equation has two $N\times N$ matrix-valued Jost solutions which allow one to construct the Jost matrix $F(k)$ defining both scattering and bound-state properties. The scattering matrix, which is symmetric, reads

$$S(k) = K^{-1/2}F(-k)F^{-1}(k)K^{1/2} = K^{1/2}[F^{-1}(k)]^T F^T(-k)K^{-1/2}, \tag{4}$$

with T meaning transposition and $-k=\{-k_1,\ldots,-k_N\}$. The zeros of the determinant of the Jost matrix, which are defined by $\det F(k)\equiv 0$, thus correspond to poles of all the elements of the scattering matrix. Bound states correspond to such zeros k_m, with $m=1,\ldots,M$, lying on the positive imaginary k_i axes for all channels: $k_{mi}=i\kappa_{mi}$ with $\kappa_{mi}\geq 0$ and $i=1,\ldots,N$. The corresponding energies $E_m=-\kappa_{mi}^2+\Delta_i$ lie below all thresholds. For simplicity, we call a virtual state any other zero of the Jost-matrix determinant corresponding to a real energy below all thresholds, but not lying on all the positive imaginary k_i axes. Finally, we call a resonance any zero of the Jost-matrix determinant not lying on the imaginary k_i axes, hence corresponding either to a complex energy or to a real energy above at least one threshold. Note that for a resonance to have a visible impact on the physical scattering matrix it should be located sufficiently close to the energy real axis above the first threshold.

Let us then summarize the main results from supersymmetric quantum mechanics in the coupled-channel case [16,17]. Starting from an initial potential V and its solutions ψ, a supersymmetric transformation allows the construction of a new potential

$$\tilde{V}(r) = V(r) - 2U'(r) \tag{5}$$

with solutions

$$\tilde{\psi}(k,r) = \left(-\frac{d}{dr} + U(r)\right)\psi(k,r), \tag{6}$$

where the so-called superpotential U is expressed in terms of a square matrix σ by

$$U(r) = \sigma'(r)\sigma^{-1}(r). \tag{7}$$

Here the prime denotes the derivative with respect to r. The matrix σ is called the factorization solution; it is a solution of the initial Schrödinger equation

$$H\sigma(r) = -\mathcal{K}^2\sigma(r), \tag{8}$$

where $\mathcal{K}=\mathrm{diag}(\kappa)=\mathrm{diag}(\kappa_1,\ldots,\kappa_N)$ is a diagonal matrix called the factorization wave number, which corresponds to an energy $\mathcal{E}$ lying below all thresholds, called the factorization energy. The entries of $\mathcal{K}$ thus satisfy $\mathcal{E}=-\kappa_i^2+\Delta_i$; by convention, we choose them positive: $\kappa_i>0$. Note that the columns of matrix σ are linearly independent vector-valued solutions of Eq. (8), none of which needs to be regular at the origin. Equation (6) implies that all the physical properties of the transformed potential can be expressed in terms of those of the initial potential, in particular its Jost and scattering matrices.

Let us now apply these results to a vanishing initial potential $V=0$, for which the Jost and scattering matrices are the identity, $S(k)=F(k)=I$. For a given factorization energy, the most general real symmetric superpotential depends on an N-dimensional real symmetric matrix of arbitrary parameters, i.e., on $N(N+1)/2$ real arbitrary parameters [15]. When $V=0$, the corresponding factorization solution can be written as

$$\sigma(r) = \cosh(\kappa r) + \mathcal{K}^{-1}\sinh(\kappa r)U_0 \tag{9a}$$

$$= (2\mathcal{K})^{-1}[\exp(\kappa r)(\mathcal{K}+U_0) + \exp(-\kappa r)(\mathcal{K}-U_0)], \tag{9b}$$

which ensures that the resulting potential $\tilde{V}$ is regular at the origin, and where the arbitrary parameters explicitly appear as the value of the (symmetric) superpotential at the origin, $U_0\equiv U(0)$; $\exp(\pm\kappa r)$, $\cosh(\kappa r)$, and $\sinh(\kappa r)$ are diagonal matrices with entries $\exp(\pm\kappa_i r)$, $\cosh(\kappa_i r)$, and $\sinh(\kappa_i r)$ respectively. According to Ref. [15], when $\mathcal{K}+U_0$ is invertible, the transformed Jost matrix reads

$$\tilde{F}(k) = (\mathcal{K}-iK)^{-1}(U_0-iK). \tag{10}$$

This is the Jost function obtained by other means in Ref. [11] in the case $q=1$. However, it was not realized there that the corresponding potential could be simply expressed in terms of a solution matrix σ, using Eqs. (5) and (7). In that reference, a compact expression for the potential is found [see Eq. (18) below] but writing (9a), (9b), and (7) is much more elegant because both the potential (5) and its Jost function (10) are expressed in terms of the same parameter matrix U_0. Nevertheless, this procedure also presents several disadvantages: calculating the potential requires several matrix operations (inversion, product, derivations); moreover, the parameters in U_0 should be chosen so that the factorization solution is invertible for all r, a condition not easily checked on Eqs. (9a) and (9b).

Let us now derive an alternative form for the factorization solution, which solves both these inconveniences. In Ref. [15], the possibility of rank $(\mathcal{K}+U_0)<N$ in Eq. (9b) has been studied, which leads to an interesting asymptotic behavior of the superpotential but which reduces the number of parameters in the model. Here, in order to keep the maximal number of arbitrary parameters in the potential, we choose $\mathcal{K}+U_0$ invertible. The factorization solution (9b) can then be multiplied on the right by $2(\mathcal{K}+U_0)^{-1}\mathcal{K}^{1/2}$, which leads to the factorization solution

$$\sigma(r) = \mathcal{K}^{-1/2}[\exp(\kappa r) + \exp(-\kappa r)X_0]. \tag{11}$$

According to Eq. (7), the superpotential, and hence the transformed potential, is unaffected by this multiplication. The

symmetric matrix X_0 now contains all the arbitrary parameters. The link between the two sets of parameters is given by

$$X_0 = \mathcal{K}^{-1/2}(\mathcal{K} - U_0)(\mathcal{K} + U_0)^{-1}\mathcal{K}^{1/2}, \tag{12}$$

$$U_0 = \mathcal{K}^{1/2}(I - X_0)(I + X_0)^{-1}\mathcal{K}^{1/2}. \tag{13}$$

Equation (11) can also be written as

$$\sigma(r) = \mathcal{K}^{-1/2}[I + X(r)]\exp(\kappa r), \tag{14}$$

where

$$X(r) = \exp(-\kappa r)X_0 \exp(-\kappa r). \tag{15}$$

With respect to writing (9a) and (9b), Eq. (14) presents several advantages. First, it allows for a simple calculation of the superpotential

$$\begin{aligned} U(r) &= \mathcal{K} - 2\mathcal{K}^{1/2}X(r)[I + X(r)]^{-1}\mathcal{K}^{1/2} \\ &= -\mathcal{K} + 2\mathcal{K}^{1/2}[I + X(r)]^{-1}\mathcal{K}^{1/2}. \end{aligned} \tag{16}$$

The last expression is particularly convenient since the r dependence is limited to one factor of the second term; the potential can thus be explicitly written as

$$\begin{aligned} \tilde{V}(r) &= 4\mathcal{K}^{1/2}[I + X(r)]^{-1}X'(r)[I + X(r)]^{-1}\mathcal{K}^{1/2} \\ &= -4\mathcal{K}^{1/2}(e^{\kappa r} + X_0 e^{-\kappa r})^{-1}(X_0\mathcal{K} + \mathcal{K}X_0) \\ &\quad \times (e^{\kappa r} + e^{-\kappa r}X_0)^{-1}\mathcal{K}^{1/2}. \end{aligned} \tag{17}$$

The last expression is exactly equivalent to Eq. (4.7) of Ref. [11] for $q=1$, which reads

$$\begin{aligned} \tilde{V}(r) &= 2e^{-\kappa r}[I - A(2\mathcal{K})^{-1}e^{-2\kappa r}]^{-1}(A\mathcal{K} + \mathcal{K}A) \\ &\quad \times [I - e^{-2\kappa r}(2\mathcal{K})^{-1}A]^{-1}e^{-\kappa r}, \end{aligned} \tag{18}$$

provided one defines matrix A as

$$A = -2\mathcal{K}^{1/2}X_0\mathcal{K}^{1/2} = -2(\mathcal{K} - U_0)(\mathcal{K} + U_0)^{-1}\mathcal{K}. \tag{19}$$

The second advantage of writing (14) is that it easily leads to a necessary and sufficient condition on the parameters to get a potential without singularity at finite distances. This condition is positive definiteness of matrix $I+X_0$:

$$I + X_0 > 0\ . \tag{20}$$

The potential has a singularity when $\sigma(r)$ is noninvertible, i.e., when $\det[I+X(r)]$ vanishes for some r. Using Eq. (15), we find that this is equivalent to the existence of $r_0 \geq 0$ such that $\det Y(r_0)=0$ with $Y(r)=\exp(2\kappa r)+X_0$. Assume now that $\det Y(r) \neq 0\ \forall\ r \geq 0$. Since $\det Y(r)=\Pi_{i=1}^{N} y_i(r)$ where $y_i(r)$ are the eigenvalues of $Y(r)$, we conclude that for all $i=1,\ldots,N$ and $r \geq 0$. But, since for sufficiently large r, X_0 becomes a small perturbation to $\exp(2\kappa r)$, all eigenvalues of $Y(r)$ should be positive for $r \geq 0$ and in particular at $r=0$, thus proving the necessary character of the above condition.

The sufficiency follows from the observation that $Y(r)$ is positive definite for any $r \geq 0$, together with $Y(0)=I+X_0$. Indeed, if $Y(r)$ is positive definite, the inequality $\langle q|Y(r)|q\rangle > 0$ holds for any $q \in L_N$. Here $\langle p|q\rangle = \Sigma_{i=1}^{N} p_i^* q_i$ is the usual inner product in the N-dimensional complex linear space L_N, with p_i and q_i being coordinates of the vectors $p,q \in L_N$ with respect to an orthonormal basis. But, since $\langle q|Y(r)|q\rangle = \langle q|X_0|q\rangle + \langle q|\exp(2\kappa r)|q\rangle \geq \langle q|X_0|q\rangle + \langle q|q\rangle = \langle q|X_0+I|q\rangle$ [we recall that $r \geq 0$, $\kappa_i > 0$, and $\exp(\kappa r)$ is a diagonal matrix with entries $\exp(\kappa_i r)$], positive definiteness of $I+X_0$ implies positive definiteness of $Y(r)$ for $r \geq 0$.

Having established this condition on X_0, one can get the condition in terms of U_0, using Eq. (12). Since

$$I + X_0 = 2\mathcal{K}^{1/2}(\mathcal{K} + U_0)^{-1}\mathcal{K}^{1/2}, \tag{21}$$

the necessary and sufficient condition to get a regular potential is positive definiteness of the matrix $\mathcal{K}+U_0$:

$$\mathcal{K} + U_0 > 0\ . \tag{22}$$

Since the (diagonal) elements of $\mathcal{K}$ are positive and increase when the factorization energy decreases, this condition has a simple interpretation: it just puts some upper limit on the factorization energy.

Finally, Eq. (19) shows that the condition $\det A \neq 0$ required in Ref. [11] is not required here. In Cox's paper, this condition does not appear in the potential expression, which is valid in the general case, but only in the derivation of the proof; the fact that this condition is not required here illustrates the efficiency of the supersymmetric formalism. Equation (19) also implies that the rank $(\mathcal{K}+U_0) < N$ corresponds to $\det A = \infty$, a case also not considered in Ref. [11]. The supersymmetric treatment, on the contrary, allows this case [14,15]; our approach thus subsumes the results of Ref. [11] in several respects.

III. GENERAL PROPERTIES OF THE 2×2 COX POTENTIAL

Having established a connection between the Cox potential and supersymmetric quantum mechanics, we now proceed to a more detailed analysis of its properties for the simplest particular case $N=2$. As it happens, this case is not only complicated enough to deserve a dedicated analysis, but also sophisticated enough to make the solution of several interesting inverse problems possible [18].

A. Explicit expression of the potential

For $N=2$, the arbitrary parameters entering the Cox potential are the entries of the superpotential matrix at the origin,

$$U_0 \equiv U(0) = \begin{pmatrix} \alpha_1 & \beta \\ \beta & \alpha_2 \end{pmatrix}, \tag{23}$$

and the factorization energy $\mathcal{E}$. The corresponding factorization wave number $\kappa=(\kappa_1,\kappa_2)$ is made up of two positive parameters κ_1 and κ_2 which are not independent of each other: they should satisfy the "threshold condition" [see Eq. (3)]

$$\kappa_2^2 - \kappa_1^2 = \Delta. \tag{24}$$

Here and in what follows we put for convenience $\Delta_1=0$, $\Delta_2=\Delta>0$.

In terms of these parameters, the necessary and sufficient condition for a regular potential, i.e., $\mathcal{K}+U_0$ positive definite, can be written, for instance,

$$\kappa_1 > -\alpha_1, \tag{25a}$$

$$\kappa_2 > \frac{\beta^2}{\kappa_1+\alpha_1} - \alpha_2. \tag{25b}$$

This puts an upper limit on the factorization energy in terms of the parameters appearing in U_0.

Two explicit expressions for the superpotential are given in Ref. [15]. Using Eqs. (5) and (16), one gets what is probably the simplest possible explicit expression for the potential itself:

$$\tilde{v}_{11} = -8\kappa_1 e^{-2\kappa_1 r}\frac{x_{11}\kappa_1 + [2x_{11}x_{22}\kappa_1 - x_{12}^2(\kappa_1+\kappa_2)]e^{-2\kappa_2 r} + x_{22}(x_{11}x_{22}-x_{12}^2)\kappa_1 e^{-4\kappa_2 r}}{[1+x_{11}e^{-2\kappa_1 r}+x_{22}e^{-2\kappa_2 r}+(x_{11}x_{22}-x_{12}^2)e^{-2(\kappa_1+\kappa_2)r}]^2}, \tag{26a}$$

$$\tilde{v}_{12} = -4x_{12}\sqrt{\kappa_1\kappa_2}e^{-(\kappa_1+\kappa_2)r}\frac{\kappa_1+\kappa_2+x_{11}(\kappa_2-\kappa_1)e^{-2\kappa_1 r}+x_{22}(\kappa_1-\kappa_2)e^{-2\kappa_2 r}-(x_{11}x_{22}-x_{12}^2)(\kappa_1+\kappa_2)e^{-2(\kappa_1+\kappa_2)r}}{[1+x_{11}e^{-2\kappa_1 r}+x_{22}e^{-2\kappa_2 r}+(x_{11}x_{22}-x_{12}^2)e^{-2(\kappa_1+\kappa_2)r}]^2}. \tag{26b}$$

The element $\tilde{v}_{22}$ is obtained from Eq. (26a) by the replacement $\kappa_1 \leftrightarrow \kappa_2$ and $x_{11} \leftrightarrow x_{22}$. Here, we have used the symmetric matrix

$$X_0 = \begin{pmatrix} x_{11} & x_{12} \\ x_{12} & x_{22} \end{pmatrix}, \tag{27}$$

which is related to matrix (23) by Eqs. (12) and (13). In the following, as we are mostly interested in the Jost-matrix properties, we shall rather use matrix U_0.

B. Zeros of the Jost-matrix determinant

Let us denote for convenience the channel wave numbers as $k_1=k$ and $k_2=p$, with the threshold condition

$$k^2 - p^2 = \Delta. \tag{28}$$

Then, according to Eq. (10), the Jost matrix for the Cox potential reads (see also Refs. [11,14,15])

$$\tilde{F}(k,p) = \begin{pmatrix} \dfrac{k+i\alpha_1}{k+i\kappa_1} & \dfrac{i\beta}{k+i\kappa_1} \\ \dfrac{i\beta}{p+i\kappa_2} & \dfrac{p+i\alpha_2}{p+i\kappa_2} \end{pmatrix}. \tag{29}$$

The determinant of the Jost matrix coincides with the Fredholm determinant of the corresponding integral equation [12]; it reads here

$$f(k,p) \equiv \det \tilde{F}(k,p) = \frac{(k+i\alpha_1)(p+ia_2)+\beta^2}{(k+i\kappa_1)(p+i\kappa_2)}. \tag{30}$$

The zeros of this Jost determinant in the k and p complex planes, which correspond to bound, virtual, or resonant states, are functions of the parameters α_1, α_2, and β only. From this and the threshold condition (28) follows the system of equations for finding the zeros of $f(k,p)$,

$$k^2 - p^2 = \Delta, \tag{31a}$$

$$(k+i\alpha_1)(p+i\alpha_2)+\beta^2 = 0, \tag{31b}$$

which is equivalent to the fourth-order algebraic equation:

$$k^4 + ia_1k^3 + a_2k^2 + ia_3k + a_4 = 0, \tag{32}$$

where

$$a_1 = 2\alpha_1, \tag{33a}$$

$$a_2 = \alpha_2^2 - \alpha_1^2 - \Delta, \tag{33b}$$

$$a_3 = 2[\alpha_1(\alpha_2^2-\Delta) - \alpha_2\beta^2], \tag{33c}$$

$$a_4 = -\alpha_1^2(\alpha_2^2-\Delta) + 2\alpha_2\beta^2\alpha_1 - \beta^4. \tag{33d}$$

We notice that, after the substitution $k=i\lambda$, Eq. (32) becomes an algebraic equation in λ with real coefficients. Its four roots are thus either real numbers, which correspond to real negative energies (bound or virtual states), or mutually conjugated complex numbers, which correspond to mutually conjugated complex energies (resonant states). Based on this property, we will use in what follows a geometric representation of the system of equations which allows for a visualization of the zeros of $f(k,p)$ in the parameter space.

Let us first consider bound and virtual states, which correspond to solutions of system (31a) and (31b) with k and p purely imaginary. After the substitutions $k=i\lambda$, $p=i\rho$, with λ and ρ real, these equations define two hyperbolas in the (λ,ρ) plane,

$$\rho^2 - \lambda^2 = \Delta\ , \tag{34a}$$

$$(\lambda+\alpha_1)(\rho+\alpha_2) = \beta^2, \tag{34b}$$

the positions of which are defined by the values of the parameters α_1, α_2, β, and Δ. The roots of system (34a) and (34b) that correspond to bound and virtual states are the intersection points of these hyperbolas. Different possibilities

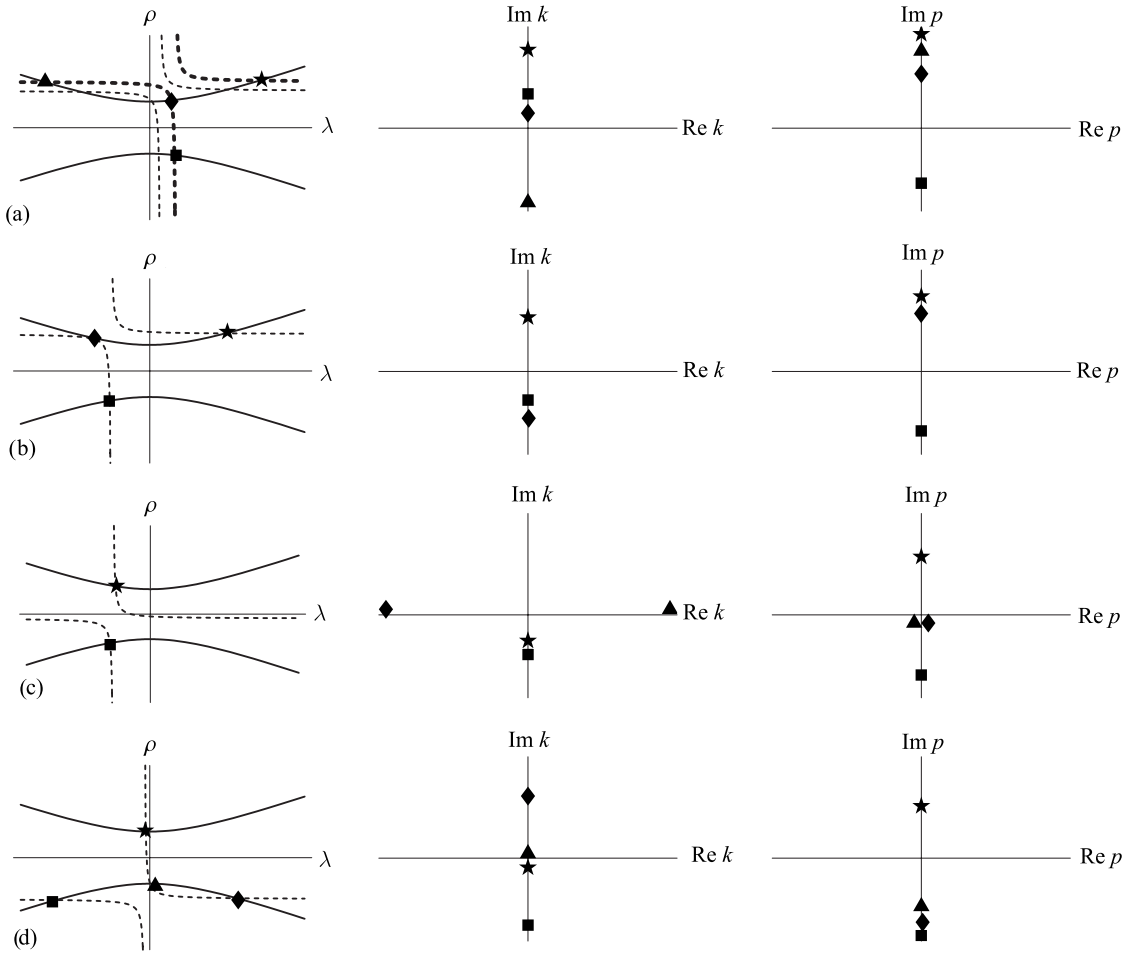

FIG. 1. Geometrical representation of Eqs. (34a) (first column, solid lines) and (34b) (first column, dashed lines), and positions of the corresponding roots of system (31a) and (31b) in the complex k (second column) and p (third column) planes. Various values of the parameters α_1 and α_2 are chosen, which imply various numbers of bound, virtual, and resonant states: (a) $\alpha_1<0$, $\alpha_2<-\sqrt{\Delta}$, two bound states (star and diamond), two virtual states (square and triangle), no resonance; (b) $\alpha_1>0$, $\alpha_2<-\sqrt{\Delta}$, one bound state (star), one virtual state (square), appearance of a resonance (diamond); (c) $\alpha_1>0$, $\alpha_2\geq 0$, no bound state, two virtual states (star and square), one resonance (triangle and diamond, not seen in the first column); (d) $\alpha_1>0$, $\alpha_2>\sqrt{\Delta}$, no bound state, no resonance, four virtual states. Increase of either α_1 or α_2 leads to (a) (thin dashed lines) disappearance of a bound state; (b) appearance of the resonance.

of hyperbola locations are shown in Fig. 1. The solid-line hyperbola corresponds to the threshold condition (34a); its semimajor axis is $\sqrt{\Delta}$ and its slant asymptotes are given by $\rho=\pm\lambda$. The dashed-line hyperbola corresponds to Eq. (34b); its asymptotes are given by $\lambda=-\alpha_1$ and $\rho=-\alpha_2$. The abscissa (ordinate) of a crossing point in the (λ,ρ) plane gives the position of the corresponding zero on the imaginary axis in the k plane (p plane), as shown in the second (third) column of Fig. 1. Bound states correspond to $\lambda,\rho>0$, i.e., to intersection points lying in the first quadrant of the (λ,ρ) plane, while virtual states correspond to intersections in the second, third, and fourth quadrants. In both cases, their energy with respect to the first threshold is given by

$$E=k^2=-\lambda^2. \tag{35}$$

It is clearly seen on Fig. 1 that the two hyperbolas (34a) and (34b) cross in either two or four points. Moreover, they can have zero, one, or two intersections in the first quadrant, which means that the potential has either zero, one, or two bound states. This contradicts Ref. [11], where it is said that the potential never supports bound states. Since Eq. (32) is fourth order, when the hyperbolas cross in four points, the Jost determinant does not have any other zero; on the other hand, when the hyperbolas cross in only two points, the Jost determinant has two other zeros, which have to form a mutually conjugated complex pair, as seen above. This last case corresponds to a resonance, as illustrated by Fig. 1(c), where the hyperbolas have only two intersection points in the (λ,ρ) plane and a pair of complex roots appears in the complex k and p planes. The potential thus has either zero or one resonance. The intermediate case of three intersection points for the hyperbolas [Fig. 1(b)] corresponds to the presence of a multiple root of Eq. (32), which lies in an unphysical sheet ($\mathrm{Im}\,k<0$, $\mathrm{Im}\,p>0$ or $\mathrm{Im}\,k>0$, $\mathrm{Im}\,p<0$) of the Riemann energy surface; this case corresponds to a transition between a one-resonance and a two-virtual-state situation.

One sees that the parameters α_1 and α_2 determine the position of hyperbola (34b) and, hence, the number of bound states n_b (0, 1, or 2) and of resonances n_r (0 or 1). Let us now determine, for fixed values of β and Δ, the domains in the plane of parameters $\mathbb{A}=(\alpha_1,\alpha_2)$ with constant values of n_b and n_r. To find domains in $\mathbb{A}$ where the system (34a) and (34b) has two complex conjugated roots (one resonance), we consider the case where the hyperbolas have a common tangent point, as illustrated by Fig. 1(b). One can see that the decrease of either α_1 or α_2 leads to the disappearance of the resonance, while the increase of either α_1 or α_2 leads to the appearance of the resonance. We define the parametric curves $[\alpha_1(\lambda_0,\rho_0),\alpha_2(\lambda_0,\rho_0)]$ in plane $\mathbb{A}$ by shifting the tangent point (λ_0,ρ_0) along the hyperbola $\rho^2-\lambda^2=\Delta$. These curves limit domains in $\mathbb{A}$ with either zero or two complex roots. To find them, we use the two conditions corresponding to the common tangent point (λ_0,ρ_0),

$$\rho_0=\frac{\beta^2}{\lambda_0+\alpha_1}-\alpha_2=\pm\sqrt{\lambda_0^2+\Delta}, \tag{36a}$$

$$\left.\frac{d\rho}{d\lambda}\right|_{\lambda=\lambda_0}=-\frac{\beta^2}{(\lambda_0+\alpha_1)^2}=\pm\frac{\lambda_0}{\sqrt{\lambda_0^2+\Delta}}. \tag{36b}$$

The upper signs correspond to $\lambda_0<0$ (tangent point in the second quadrant) while the lower signs correspond to $\lambda_0>0$ (tangent point in the fourth quadrant). We can solve system (36a) and (36b) with respect to α_1 and α_2:

$$\alpha_1(\lambda_0)=\pm\frac{\beta}{\sqrt{|\lambda_0|}}(\lambda_0^2+\Delta)^{1/4}-\lambda_0, \tag{37a}$$

$$\alpha_2(\lambda_0)=\pm\frac{\beta\sqrt{|\lambda_0|}}{(\lambda_0^2+\Delta)^{1/4}}+\mathrm{sgn}(\lambda_0)\sqrt{\lambda_0^2+\Delta}. \tag{37b}$$

It should be noted that the Schrödinger equation with the Cox potential has the following scale invariance:

$$\alpha_{1,2}\to\gamma\alpha_{1,2},\quad \Delta\to\gamma^2\Delta, \tag{38a}$$

$$\kappa_{1,2}\to\gamma\kappa_{1,2},\quad \beta\to\gamma\beta, \tag{38b}$$

$$r\to r/\gamma, \tag{38c}$$

which leaves $\Delta_d=\Delta/\beta^2$ invariant. Hence, we may put $\Delta=1$ without losing generality. This choice is equivalent to measuring energies in units of Δ. It is convenient to express Eqs. (37a) and (37b) in terms of dimensionless variables α_i/β, $\Delta_d=\Delta/\beta^2$, $\lambda_0\to\lambda_0/\beta$:

$$\frac{\alpha_1}{\beta}(\lambda_0)=\pm\frac{1}{\sqrt{|\lambda_0|}}(\lambda_0^2+\Delta_d)^{1/4}-\lambda_0, \tag{39a}$$

$$\frac{\alpha_2}{\beta}(\lambda_0)=\pm\frac{\sqrt{|\lambda_0|}}{(\lambda_0^2+\Delta_d)^{1/4}}+\mathrm{sgn}(\lambda_0)\sqrt{\lambda_0^2+\Delta_d}. \tag{39b}$$

These four solutions [taking into account $\mathrm{sgn}(\lambda_0)$] can be considered as four parametric curves in the plane $\tilde{\mathbb{A}}=(\alpha_1/\beta,\alpha_2/\beta)$, which separate the plane into five regions (one inner region and four outer regions; see Fig. 2).

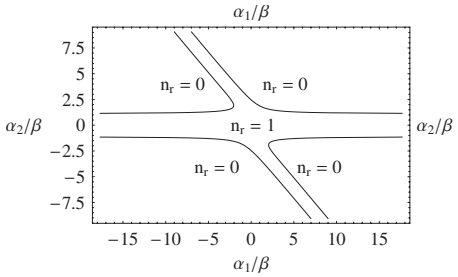

FIG. 2. Parametric curves in terms of dimensionless parameters defined by Eqs. (39a) and (39b) in the plane $\tilde{\mathbb{A}}=(\alpha_1/\beta,\alpha_2/\beta)$ for $\Delta/\beta^2=1.2$. The left-hand-side curves correspond to the lower signs in the equations, while the right-hand-side curves correspond to the upper signs. The number of resonances, n_r, is indicated in each domain of the plane.

In the inner region, the Jost determinant has two complex roots $k_{1,2}=\pm k_r+ik_i$ and, hence, these values of parameters α_1,α_2 correspond to one resonance $(n_r=1)$. In this case, we define the resonance energy with respect to the first threshold E_r and the resonance width Γ by

$$k_{1,2}^2=E_r\pm i\Gamma/2. \tag{40}$$

In the four outer regions, the Jost determinant has purely imaginary roots; hence $n_r=0$. The curves in Fig. 2 tend asymptotically to straight lines which are defined as the limits for $\lambda_0\to 0$ and $\lambda_0\to\pm\infty$. As a result, one finds for all branches two horizontal asymptotes $\alpha_2/\beta=\pm\sqrt{\Delta_d}$ and three slant asymptotes defined by $\alpha_2/\beta=-\alpha_1/\beta$ (for the curves in the second and fourth quadrants) and $\alpha_2/\beta=-\alpha_1/\beta\pm 2$ (for the curves in the first and third quadrants, respectively).

Consider now the case where the hyperbolas cross at the point $\lambda_0=0$, $\rho_0=\sqrt{\Delta}$ [see the thin dashed lines in Fig. 1(a)]. After a small decrease of either α_1 or α_2, the number of positive roots, i.e., of bound states, increases by one unit. Hence, assuming $\lambda_0=0$ and $\rho_0=\sqrt{\Delta}$ in system (34a) and (34b), we get the curves

$$\alpha_1(\alpha_2+\sqrt{\Delta})-\beta^2=0, \tag{41}$$

which define three domains in the plane of parameters $\mathbb{A}$, where Eqs. (34a) and (34b) have different numbers of positive roots (see Fig. 3). One can directly check that the number n_b of bound states may be calculated as a function of the parameters as

$$n_b=1+\frac{1}{2}(I_1-1)I_2, \tag{42}$$

where the quantities

$$I_1=\mathrm{sgn}(\beta^2-\alpha_1\sqrt{\Delta}-\alpha_1\alpha_2)1, \tag{43a}$$

$$I_2=\mathrm{sgn}(\alpha_2+\sqrt{\Delta})1 \tag{43b}$$

may be considered as invariants. For $n_b=0$, one has $I_1=-1$ and $I_2=1$; for $n_b=1$, one has $I_1=1$ and $I_2=\pm 1$; for $n_b=2$, one has $I_1=I_2=-1$.

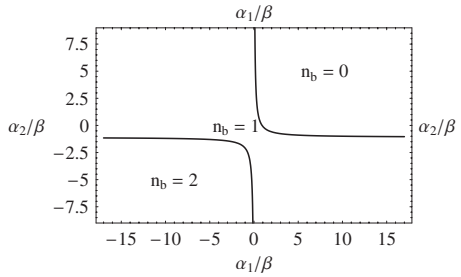

FIG. 3. Curves (41) in plane $\tilde{\mathbb{A}}$ in terms of dimensionless parameters for $\Delta/\beta^2=1.2$. The number of bound states, n_b, is indicated in each domain of the plane.

Let us now summarize our findings on the number of bound states and resonances of the 2×2 Cox potential, by combining Figs. 2 and 3 in Fig. 4, where both n_b and n_r are given for all the possible regions of plane $\tilde{\mathbb{A}}$. The border lines of these regions, as already discussed, correspond to the parametric curves defined by Eqs. (37a), (37b), (39a), and (39b), and to the curves given by Eq. (41). From the asymptotic behavior of these curves, it is easy to see the global structure of the zones. For instance, for the case of two bound states, the hyperbolas in Fig. 1 have to have four intersection points, which implies that no resonance is present. This is the reason why the boundary lines between the zones of bound and resonant states do not cross in the lower half $\tilde{\mathbb{A}}$ plane. Moreover, one can see that the topological structure of these zones does not depend on a particular choice of the parameter $\Delta_d=\Delta/\beta^2$. A change of this parameter leads only to a deformation of zones, namely, the distance between horizontal asymptotes changes, but does not make any new intersection point or new boundary line appear.

The case of $\beta=0$, $\Delta_d=\infty$ corresponds to uncoupled channels. In this case there are no resonances. Only bound or virtual states located in different channels may appear (see Sec. IV A).

Up to now, we have excluded the factorization energy from our analysis because Eqs. (34a) and (34b) are independent of $\kappa_{1,2}$, but conditions (25a) and (25b) put an upper limit on κ_1 (κ_2). The allowed values of κ_1 should be such that $\kappa_1>\sqrt{|E_g|}$, where E_g is the ground-state energy if it is present and $E_g=0$ otherwise (for details, see Ref. [18]). The necessary and sufficient condition for a regular potential can thus be simply stated: the factorization energy should be negative and lower than the ground-state energy, if any.

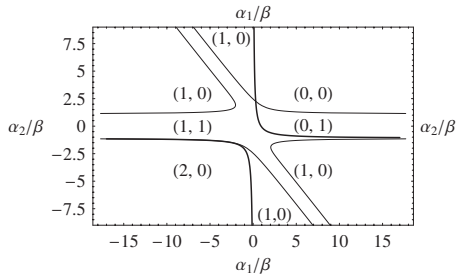

FIG. 4. Regions of the $\tilde{\mathbb{A}}$ plane with different numbers of bound states and resonances, (n_b,n_r), for the Cox potential with $\Delta/\beta^2=1.2$.

To conclude our consideration of the zeros of the Jost matrix determinant we note that, for solving a realistic two-channel scattering inverse problem, it is necessary to express the Cox potential in terms of physical data such as the threshold energy, bound-state energies, resonance energy and width, or scattering data. While the threshold energy explicitly appears in the expression of the Cox potential as the parameter Δ, the other data are directly related to the positions of the zeros of the Jost-matrix determinant, as seen above. Ideally, one would thus like to directly express parameters α_1, α_2, β, and $\mathcal{E}$, which define the Cox potential, in terms of the roots of Eq. (32). Certainly, there exist general formulas for the roots of the fourth-order algebraic equation (32), but they are very involved and cannot help much in realizing the above program. Therefore, we propose an intermediate approach (for details, see Ref. [18]) and, with the cold atom in mind, prefer to focus on the low-energy scattering in the following section.

C. Low-energy scattering matrix

In this section, we analyze the S matrix given by Eq. (4) for energies close to the lowest threshold, the energy of which we have chosen equal to zero. From Eqs. (29) and (30), one finds the Cox-potential S matrix

$$\mathbf{S}(k,p)=\frac{1}{f(k,p)}\begin{pmatrix} f(-k,p) & \dfrac{-2i\beta\sqrt{kp}}{k^2+\kappa_1^2} \\ \dfrac{-2i\beta\sqrt{kp}}{p^2+\kappa_2^2} & f(k,-p) \end{pmatrix}. \tag{44}$$

When the second channel is closed, i.e., for energies $0<E<\Delta$, the physical scattering matrix is just a function $S(k,p)$, which coincides with the first diagonal element of S matrix (44). It reads

$$S(k,p)=\frac{k+i\kappa_1}{k-i\kappa_1}\frac{[i(k-i\alpha_1)(\sqrt{\Delta-k^2}+\alpha_2)-\beta^2]}{[i(k+i\alpha_1)(\sqrt{\Delta-k^2}+\alpha_2)+\beta^2]}. \tag{45}$$

From here one finds the scattering amplitude $A(k)=[S(k)-1]/2ik$, which reads

$$A(k)=\frac{(\alpha_2+\sqrt{\Delta-k^2})(\alpha_1-\kappa_1)-\beta^2}{i(k-i\kappa_1)[i(k+i\alpha_1)(\sqrt{\Delta-k^2}+\alpha_2)+\beta^2]}, \tag{46}$$

and the scattering length $a=-A(0)$, which reads

$$a=\frac{1}{\kappa_1}+\frac{\sqrt{\Delta}+\alpha_2}{\beta^2-\alpha_1(\sqrt{\Delta}+\alpha_2)}. \tag{47}$$

From the argument of $S(k)=e^{2i\delta(k)}$, one deduces the phase shift $\delta(k)$, which reads

$$\delta(k) = \arctan\frac{k}{\kappa_1} + \arctan\frac{k(\sqrt{\Delta - k^2} + \alpha_2)}{\beta^2 - \alpha_1(\sqrt{\Delta - k^2} + \alpha_2)}. \quad (48)$$

One can check in Eqs. (47) and (48) that the scattering length is the slope of the phase shift at zero energy, as it should be. Note that Eq. (48) is equivalent to

$$k \cot \delta(k) = \frac{a_\beta(k)\kappa_1 + k^2}{\kappa_1 - a_\beta(k)}, \quad (49)$$

where $a_\beta(k) = \alpha_1 - \beta^2/(\sqrt{\Delta - k^2} + \alpha_2)$. In the uncoupled case ($\beta = 0$), this expression reduces to the phase shifts of the simplest Bargmann potential (see, e.g., Ref. [12]), which depends on the parameters κ_1 and $a_B \equiv a_{\beta=0} = \alpha_1$. Therefore, the Cox potential may be considered as a coupled-channel deformation of the Bargmann potential, resulting in an energy dependence of one of its parameters, a_B.

The scattering length is an important physical quantity. In many-body theories for instance, it is often used to describe interactions in the s-wave regime. Let us thus study in detail the scattering length of the Cox potential, as given by Eq. (47). When considered as a function of $\alpha_{1,2}$, it has a singularity located at the boundary of the single-bound-state region provided by Eq. (41). Such infinite values of the scattering length happen when a zero of the Jost determinant, which corresponds to an S-matrix pole, crosses the first threshold: a bound state is then transformed into a virtual state, in agreement with the general theory [12].

IV. TWO-CHANNEL MODEL OF ALKALI-METAL ATOM-ATOM COLLISIONS IN THE PRESENCE OF A MAGNETIC FIELD

A. Magnetic Feshbach resonance

Ultracold collisions of alkali-metal atoms play a key role in applications of laser cooling such as Bose-Einstein condensation (BEC) and the BEC-BCS crossover. The analysis of such experiments is commonly based on the coupled-channel method [19], i.e., on solving numerically a set of coupled differential equations.

In this paper, we reduce the low-energy scattering problem of two alkali-metal atoms to an effective two-channel problem with a single Feshbach resonance, as in Ref. [8]. The model consists of a single closed channel Q containing a bound state, which interacts with the scattering continuum in the open channel P, so that the whole scattering problem is reduced to the two-channel scattering described by the 2×2 Hamiltonian

$$H = -\frac{d^2}{dr^2} + \begin{pmatrix} V_P(r) & V_{\text{int}}(r) \\ V_{\text{int}}(r) & V_Q(r) \end{pmatrix}, \quad (50)$$

where V_P is the uncoupled open-channel potential, V_Q is the uncoupled closed-channel potential, and potential V_{int} describes the coupling between the open and closed channels P and Q. These channels describe atoms placed in a magnetic field and occupying different energy sublevels, which can be shifted with respect to each other with a change of the magnetic field (Zeeman effect). For each value of the magnetic field, the zero of energy is chosen as the energy of the dissociated atoms in channel P.

Even in the simplest case of a homogeneous magnetic field, the potential-energy matrix of Hamiltonian (50) depends on the magnetic field. We will assume that the external field changes slowly enough so that we can take advantage of the adiabatic approximation, assuming that the stationary Schrödinger equation may be applied for describing the scattering process and the magnetic field enters the Hamiltonian as a parameter only. Moreover, the known observation that, when the scattering length is much larger than the range of the interaction, the general behavior of the system is nearly independent of the exact form of the potential [20], suggests that we use the Cox potential with large scattering length for describing the interatomic scattering. We thus replace the potential matrix in Eq. (50) by the Cox potential. In this case, the parameters of the Cox potential should carry a dependence on the magnetic field. Below, we show that, to get a good agreement with available experimental data, it is sufficient to impose a linear field dependence on the threshold difference Δ only, keeping all other parameters field independent. Thus, inverting known scattering experimental data, one can find all the parameters defining the Cox potential, obtaining in this way a simple analytical model of the atom-atom scattering process in the presence of a magnetic field.

The position of the highest bound (or virtual) state is crucial in describing the resonance phenomena of interatomic collisions. In an s-wave single-channel system, the scattering process becomes resonant at low energy when a bound or virtual state is located near the threshold, a phenomenon known as potential resonance. In a multichannel system, the incoming channel (which is always open) may be coupled during the collision process to other open or closed channels, corresponding to different spin configurations. When a bound state in a closed channel lies near the collision energy continuum, a Feshbach resonance [1,2] may occur, giving rise to scattering properties that are tunable by an external magnetic field. In Ref. [7], some interesting examples of the interplay between a potential resonance and a Feshbach resonance are considered. Below, we adjust the analytically solvable model based on the Cox potential for describing the same phenomena.

Typically, the coupling between the closed and open channels is rather small; we thus consider first an uncoupled limit of the Cox potential, i.e., $V_{\text{int}}(r) \to 0$, which corresponds to $\beta \to 0$. In this case, the Jost determinant (30) has the following zeros:

$$k_{1,2} = -i\alpha_1, \quad p_{1,2} = \pm i\sqrt{\alpha_1^2 + \Delta}, \quad (51)$$

and

$$p_{3,4} = -i\alpha_2, \quad k_{3,4} = \pm i\sqrt{\alpha_2^2 - \Delta}. \quad (52)$$

According to Eq. (35), the energies of these unperturbed (i.e., with zero coupling) states (called bare molecular states in Ref. [7]) with respect to the first threshold are

$$E_P = E_{1,2} = -\alpha_1^2 \quad (53)$$

and

$$E_Q = E_{3,4} = -\alpha_2^2 + \Delta. \tag{54}$$

It should be noted that in this case E_P belongs to channel P while E_Q belongs to channel Q. Hence, α_1 is associated with the potential resonance, while α_2 is associated with the Feshbach resonance. Due to the Zeeman effect, the difference between the thresholds is a linear function of the magnetic field,

$$\Delta(B) = \Delta_0 + \mu_{\text{mag}}(B - B_0), \tag{55}$$

where B_0 can be arbitrarily chosen in the domain of interest and Δ_0 is the value of the threshold corresponding to B_0. If $\alpha_{1,2} < 0$ and the coupling is absent, then the two bound states cross at $\Delta = \alpha_2^2 - \alpha_1^2$. Note that E_Q crosses the threshold at $\Delta = \alpha_2^2$. When there is a coupling between channels, the levels E_P and E_Q avoid crossing (see below).

Let us consider the behavior of the scattering length in the presence of the Feshbach resonance. It is described by the following formula [5]:

$$a = a_{\text{bg}}\left(1 - \frac{\Gamma_B}{B - B_0}\right). \tag{56}$$

Here, B_0 is the position of the magnetic Feshbach resonance and Γ_B is its width (in terms of magnetic field).

In particular, Eq. (47) shows that such an infinite value of the scattering length occurs for the Cox potential at a threshold Δ_0 defined by

$$\sqrt{\Delta_0} = \frac{\beta^2 - \alpha_1\alpha_2}{\alpha_1}. \tag{57}$$

Let us now assume for the Cox potential a threshold difference given by Eq. (55) with such a value of Δ_0. Expanding Eq. (47) near this resonance one gets

$$a = \frac{\alpha_1 - \kappa_1}{\alpha_1\kappa_1}\left(1 + \frac{2\left[1 + \dfrac{\Delta - \Delta_0}{2\Delta_0} + \cdots\right]\kappa_1\sqrt{\Delta_0}(\sqrt{\Delta_0} + \alpha_2)}{(\alpha_1 - \kappa_1)(\Delta_0 - \Delta)}\right), \tag{58}$$

which has the form (56) with the width

$$\Gamma_B = \frac{2\kappa_1\sqrt{\Delta_0}(\sqrt{\Delta_0} + \alpha_2)}{\mu_{\text{mag}}(\alpha_1 - \kappa_1)}, \tag{59}$$

and the background scattering length

$$a_{\text{bg}} = \frac{1}{\kappa_1} - \frac{1}{\alpha_1}. \tag{60}$$

As shown in Ref. [7], the background scattering length a_{bg} is due to the open-channel potential. Indeed, Eqs. (47) and (60) show that, for our model, $a_{\text{bg}} = \lim_{\beta\to 0} a$. When there is a bound or virtual state close to threshold, it can be further decomposed as a sum of two contributions: a standard potential part, which depends on the potential range, and a potential-resonance part, which depends on the bound- or virtual-state energy. This decompostion clearly appears in our model: in formula (60), the first term is proportional to $1/\kappa_1$, the parameter that defines the range of the open-channel potential [see Eqs. (26a) and (26b)]; it may thus be considered as the standard potential part of the background scattering length. The second term is associated with the P-channel bound (or virtual) state in the uncoupled limit. Hence, it may be interpreted as the potential-resonance part of the background scattering length. Let us further consider two different possibilities giving rise to a large (either positive or negative) background scattering length.

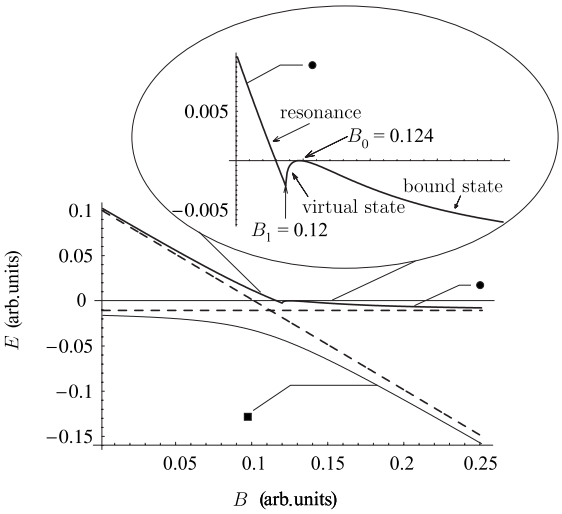

FIG. 5. Energies of bare (dashed lines) and dressed (solid lines) states as functions of the magnetic field B for the Cox potential defined by parameters (61a)–(61d). The transition between a Feshbach resonance, a virtual state, and a bound state is shown in the inset for the ● solid line. The dressed ground state is shown by the ■ solid line.

B. Interplay between a bound state and the Feshbach resonance

The first possibility occurs when the highest bound state is located near the threshold, i.e., when $\alpha_1 \lesssim 0$. In Fig. 5, we show energies as functions of the magnetic field when channel P has a bound state just below the threshold, for

$$\beta = 0.05, \tag{61a}$$

$$\alpha_1 = -\lambda_b = -0.103, \tag{61b}$$

$$\alpha_2 = -0.5, \tag{61c}$$

$$\kappa_1 = 1. \tag{61d}$$

Without coupling between the channels ($\beta = 0$), the energies $E = k^2$ of the bare bound states with respect to the first threshold are shown in Fig. 5 by the dashed horizontal [see Eq. (53)] and slanted [see Eq. (54)] lines respectively, as functions of the magnetic field B. We are using arbitrary units and choose $\Delta(B) = 0.35 - B$ in Eq. (55).

For the coupled case, the B-behavior of the (dressed) ground state is shown by the ■ solid line and it now avoids crossing with the (dressed) excited state (cf. [7]) which is shown by the ● solid line.

For the fields $B > 0$ and up to a value $B = B_1$ (which we define below), the excited bare state in Q space becomes a

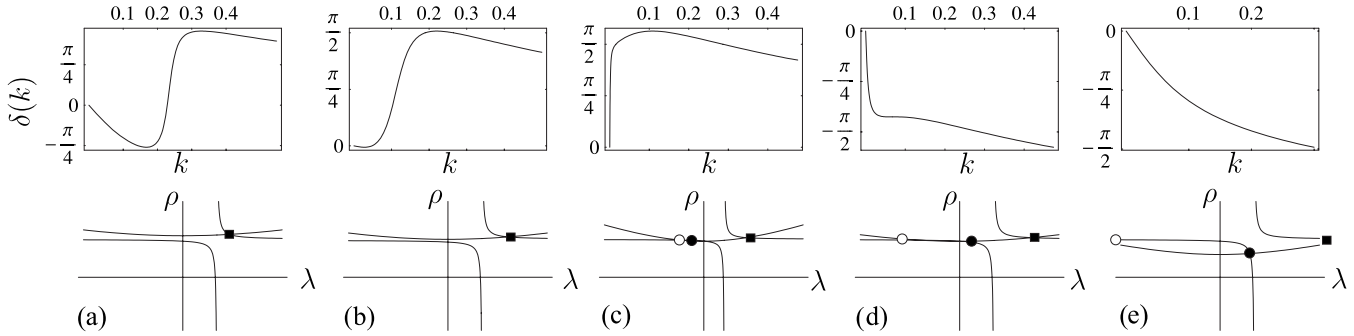

FIG. 6. Phase shifts and graphical representation of Eqs. (34a) and (34b) for the Cox potential defined by parameters (61a)–(61d). The ■ corresponds to the position of the dressed ground state. The ● corresponds to the virtual state which transforms into a bound state. The ○ corresponds to the virtual state. The columns correspond to different values of the magnetic field: $B=$ (a) 0.05; (b) 0.1; (c) 0.1235; (d) 0.125; (e) 0.24.

resonance and the corresponding Jost determinant zero shifts from the real axis in the k plane to the lower half of the complex k plane and from the imaginary axis in the p plane it shifts to the upper half plane. Recall that, according to our convention (40), we show the real part of k^2 for the resonance in Fig. 5, which may be negative. For any complex zero of the Jost determinant there exists another zero with the opposite sign of the real part. With the growth of B, these two zeros move toward each other, approaching the imaginary axis from different sides, where they merge, thus defining the point $B=B_1=0.12$. At this point the zeros become purely imaginary [● and ○ in Figs. 6(c)–6(e)] which corresponds to appearance of two virtual states and the discontinuous slope of the real part of the energy clearly visible in Fig. 5. With further increase of the magnetic field, one of these virtual states (● solid line in Fig. 5 and ● in Fig. 6) tends to the threshold, while the other virtual state (not represented in Fig. 5, ○ in Fig. 6) goes down along the imaginary axis. At $B_0=0.124$, the virtual state crosses the threshold and becomes a bound state; the scattering length thus goes through infinite values at that field: this is the magnetic-Feshbach-resonance phenomenon itself. Above B_0, the model has two bound states, the energies of which tend to the bare-state energies when the field continues to increase.

Following Ref. [7], we stress that, although the behavior of the dressed states shows some resemblance to the two-level Landau-Zener description, this model does not include the threshold effects shown in Fig. 5 and, hence, cannot be used to properly describe the interplay between a potential resonance and a Feshbach resonance. With respect to Ref. [7], our model displays a slightly more sophisticated behavior for the state energies (compare our Fig. 5 with their Fig. 4). A more significant difference of our description is the direct knowledge of the coupled-channel potential corresponding to these energies. This potential is shown in Fig. 7 for $B=0.1$. The potential form factor changes slowly with the change of the magnetic field, which is mainly responsible for the variation of Δ.

The value of κ_1 chosen in Eq. (61d) is arbitrary. However, the necessary and sufficient condition to get a Cox potential without singularity requires then that the bound-state energies of the model should be larger than -1. Figure 5 shows that this condition will be satisfied for a limited range of magnetic field only. For higher fields, a larger κ_1 should be chosen.

The phase shifts of the same Cox potential, as well as a graphical representation of Eqs. (34a) and (34b), are shown in Fig. 6 for different values of B. The first and the last columns correspond to a large positive background scattering length ($a_{\mathrm{bg}}\sim 1/\lambda_b\approx 10$), due to a bound state close to the threshold.

Physically, this occurs for the ^{133}Cs atom-atom interaction [21], for instance. Figure 6(b) illustrates the case where the scattering length is close to zero. The calculation or measurement of the zero of the scattering length plays an important role in determining the resonance width [22]. The phase-shift behavior for the virtual state and bound state close to threshold is shown in Figs. 6(c) and 6(d), respectively. In this case, the scattering length is very large and its sign changes while the energy of the zero of the Jost-matrix determinant crosses the threshold. Recalling that the intersection points in the graphical representation of Eqs. (34a) and (34b), shown in the second row of Fig. 6, give the positions of bound and virtual states, one may establish a correspondence between the second row of Fig. 6 and the motion of the corresponding zeros in the complex plane described above.

C. Interplay between a virtual state and the Feshbach resonance

Another interesting possibility occurs when there is a virtual state close to the threshold, i.e., when $\alpha_1\gtrsim 0$. This is the

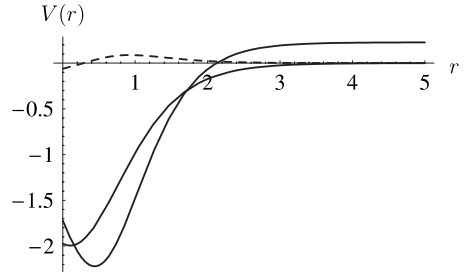

FIG. 7. Cox potential defined by parameters (61a)–(61d) for $B=0.1$; V_P and $V_Q+\Delta$ are represented by solid lines, V_{int} by a dashed line.

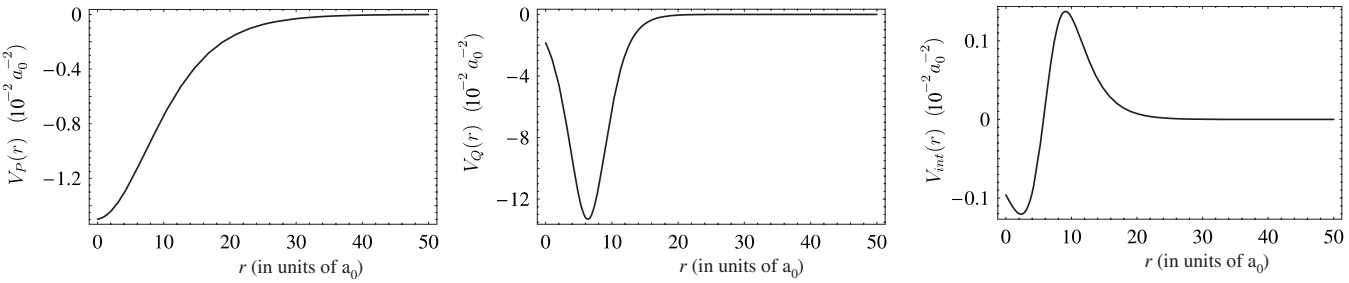

FIG. 8. Cox potential describing the Feshbach resonance in ^{85}Rb, defined by parameters (64a)–(64e), plotted at $B=14.5$ mT ($\Delta=0.059\,036\,3a_0^{-2}$).

case of the ^{85}Rb atom-atom interaction, for example. We will use rubidium scattering data [7,23] in this example, and work with units $\hbar=2\mu=1$, where μ is the reduced mass of the two atoms. The length unit is chosen as the Bohr radius a_0; energies are thus expressed in units of a_0^{-2}. According to Ref. [7], the bare virtual state is located at $\lambda_v=-1.78\times10^{-3}a_0^{-1}$, but this value is associated with the model they used in their calculations. We just consider $\lambda_v\sim-10^{-3}a_0^{-1}$ and set Eq. (60) as a constraint between $\alpha_1=-\lambda_v$ and κ_1. In order to fit the scattering-length behavior (56) with $a_{bg}=-443\ a_0$, $B_0=15.5041$ mT, and $\Gamma_B=1.071$ mT, we use Eq. (47). The value of β defines, in particular, the position of the Feshbach resonance, i.e., the magnetic field B_0 for which the bound state crosses the threshold. According to Eq. (41), one has

$$\beta=\sqrt{\alpha_1(\alpha_2+\sqrt{\Delta_0})}, \tag{62}$$

where Δ_0 is the value of the threshold corresponding to B_0. The value of α_2, defining the width of the Feshbach resonance Γ_B, should be found from the condition $a(B_0+\Gamma_B)=0$. Then, according to Eq. (47), we find

$$\alpha_2=\frac{\alpha_1[\sqrt{\Delta(B_0+\Gamma_B)}-\sqrt{\Delta_0}]}{\kappa_1}-\sqrt{\Delta(B_0+\Gamma_B)}, \tag{63}$$

where $\Delta_0=2471.386$ MHz and $\mu_{mag}=-36.4$ MHz/mT [7]. To get that value of Δ_0, we have used the known value of the threshold at zero magnetic field [23] and assumed that Eq. (55) is valid down to that field.

From Eq. (60), we may fix $\kappa_1=\alpha_1/(1+a_{bg}\alpha_1)$ at $a_{bg}=-443a_0$ and find the values of all parameters defining the potential at the given position of the Feshbach resonance and with the given value of the background scattering length:

$$\beta=0.020\,236\,6a_0^{-1}, \tag{64a}$$

$$\alpha_1=-\lambda_v=2.2\times10^{-3}a_0^{-1}, \tag{64b}$$

$$\alpha_2=-0.239\,343a_0^{-1}, \tag{64c}$$

$$\kappa_1=0.0866a_0^{-1}, \tag{64d}$$

$$\kappa_2=\sqrt{\kappa_1^2+\Delta}=\sqrt{0.078\,966\,8-0.856\,899B}a_0^{-1}. \tag{64e}$$

The value $\alpha_1=2.2\times10^{-3}a_0^{-1}$ was chosen to get a smooth potential V_P without a repulsive core. This potential is shown in Fig. 8 and, once again, has a form factor rather independent of the field, except for the threshold.

In Fig. 9, we show that, with these parameters, the Cox-potential scattering length (47) reproduces the Feshbach-resonance scattering length (56) with good precision.

The behavior of the phase shifts in the region with the resonant and virtual states is shown in the first row of Fig. 10. A similar discussion to that of Fig. 6 can be made here, except that here the large negative background scattering length results in a large positive slope for the phase shift at the origin.

Exactly at $B_0=15.5041$ mT, when the bound state transforms into a virtual state, the phase shift starts from $\pi/2$. The second row of Fig. 10 shows the corresponding behavior of the bound- and virtual-state zeros on the wave-number imaginary axes, confirming the above analysis.

Similarly to the interplay between the ground state and the Feshbach resonance discussed in detail in the previous section, Fig. 11 shows the interplay between the virtual state and the Feshbach resonance, where the corresponding energies $E=k^2$ are plotted as functions of the magnetic field B (as in the previous section, for the resonance we show Re k^2 in Fig. 11). The bare bound state of channel Q is represented by the slanted dashed line. The bare virtual state of channel P, which is located at $\lambda_v=-2.2\times10^{-3}a_0^{-1}$, is not shown in Fig. 11. The dressed states are indicated by solid lines. When $B<B_0=15.5041$ mT, there exist both a virtual state [■ in Fig. 10(a)] and a Feshbach resonance, the energies of which tend to the bare-state energies for small B. The virtual state

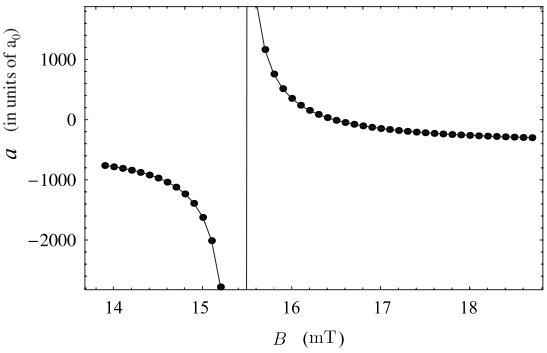

FIG. 9. Solid line: Feshbach-resonance scattering length (56) for the ^{85}Rb parameters [7,23]. Dots: Cox-potential scattering length (47) for the parameters (64a)–(64e).

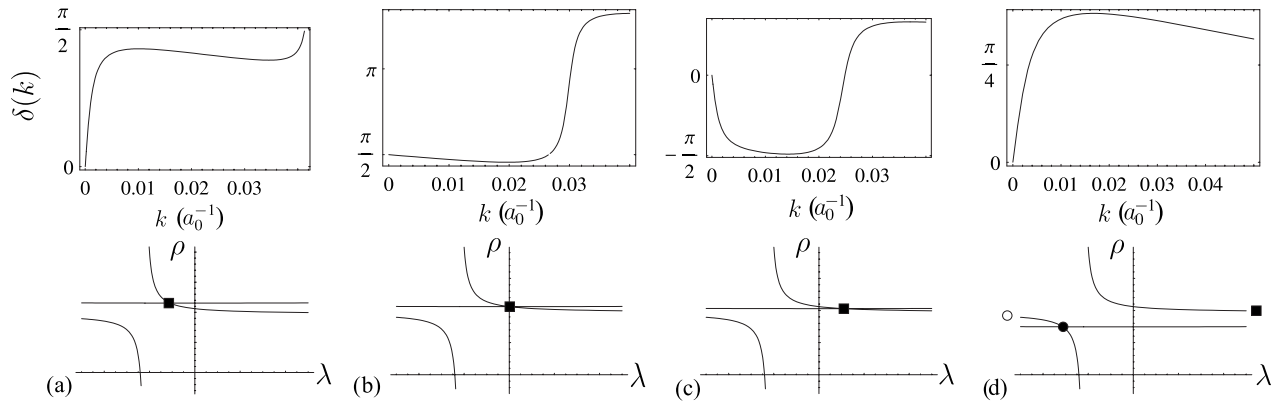

FIG. 10. Phase shifts and graphical representation of Eqs. (34a) and (34b) for the Cox potential defined by parameters (64a)–(64e). The symbols ●, ○ and ■ label positions of the Jost-determinant zeros. The columns correspond to different values of the magnetic field: (a) $B=$ (a) 14.454; (b) 15.504; (c) 15.854; (d) 19.0 mT. In the last column, ○ and ■ correspond to the zeros, which are not visible in that scale.

becomes a bound state at $B=B_0$ [see ■ solid line in the inset in Fig. 11 and Fig. 10(b)]. With increasing B, the real part of the resonance energy decreases and at $B=16.657$ mT it crosses the threshold. Finally, at $B=16.9$ mT, the two resonance zeros collapse and produce two virtual states, one of which stabilizes at $\lambda_v=-2.2\times10^{-3}a_0^{-1}$ (● in Fig. 10; the other one has a much larger negative energy and is not represented, as it does not affect the low-energy scattering properties). The behavior of the curves in Fig. 11 is very similar to those of Fig. 5, in particular regarding the transformation of the Feshbach resonance into a virtual state. The only difference between the present case (avoided crossing between a virtual state and a Feshbach resonance) and the previous case (avoided crossing between a bound state and a Feshbach resonance) is that here a virtual state transforms into a bound state before the crossing, while there a virtual state transforms into a bound state after the crossing. Another interesting comparison is between our Fig. 11 and Fig. 5 of Ref. [7]; it would be instructive to perform a detailed comparison of the two models to explain the differences between these two figures.

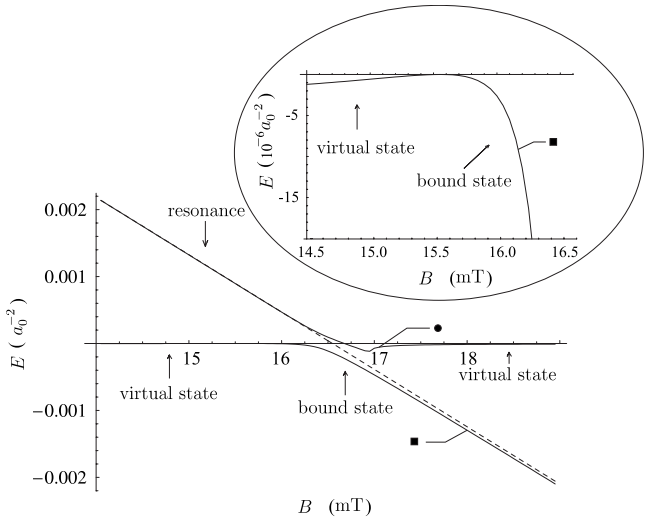

FIG. 11. B dependence of the energies of the bare (dashed lines) and dressed (solid lines) states for the Cox potential defined by parameters (64a)–(64e). The ■ solid line corresponds to the transformation from the virtual into the bound state. The ● solid line corresponds to the transformation from the resonance into the virtual state.

As for the interplay with a bound state, Fig. 11 also shows some limit on the range of magnetic field on which our model can be used: since κ_1 is fixed in Eq. (64d) and the bound-state energy should be larger than $-\kappa_1^2\approx-0.0075a_0^{-2}$ (otherwise the potential becomes singular for some value of r), the field should be lower than 24.5 mT.

V. CONCLUSION

In this work, we have derived the exactly solvable N-channel Cox potential from a supersymmetric transformation of the vanishing potential and we have established different parametrizations of this potential, as well as a necessary and sufficient condition for its regularity. In the $N=2$ case, a full analysis of the corresponding Jost matrix has been carried out. In particular, the structure of the zeros of the Jost determinant has been presented geometrically. With ultracold gases in mind, we have also studied the low energy S matrix and the scattering length of the Cox potential. Using the independence of scattering properties from interaction details in the regime with a large scattering length, a model of alkali-metal atom-atom scattering has been constructed. This provides interesting exactly solvable schematic models for the interplay of a magnetically induced Feshbach resonance with a bound or a virtual state close to threshold.

We consider the development of supersymmetric transformations as a very promising tool for the multichannel inverse scattering problem and for the construction of more advanced exactly solvable coupled-channel models. In particular, iterations or chains of transformations might lead to more complicated Jost functions, with arbitrary numbers of bound states and resonances, hopefully still with a tractable connection between potential parameters and physical observables.

As far as physical applications are concerned, atom-atom interactions are both very interesting today, due to the active research field of ultracold gases, and rather simple with re-

spect to supersymmetric quantum mechanics, as only *s* waves have to be considered and as the interaction is short ranged (no Coulomb term). We foresee applications of the present model to other systems presenting these simple features, namely, coupled *s*-wave baryon-baryon interactions, with at least one neutral baryon. In the longer term, we hope to generalize our method to higher partial waves and to Coulomb interactions. This should allow us to construct useful models in the context of low-energy nuclear reactions, the field that first motivated the work of Feshbach [1,2] on coupled-channel resonances, leading to possible applications in nuclear astrophysics and exotic-nuclei low-energy reactions.

ACKNOWLEDGMENTS

We thank Daniel Baye for very useful discussions at several stages of this work and for drawing our attention to Ref. [8]. A.P. is supported by the Russian "Dynasty" foundation. BFS is partially supported by RFBR Grant No. 06-02-16719. A.P. and B.F.S. were partially supported by Russia President Grant No. 871.2008.2; they also thank the National Fund for Scientific Research, Belgium, for support during their stays in Brussels. This text presents research results of the Belgian program P6/23 on interuniversity attraction poles of the Belgian Federal Science Policy Office (BriX, Belgian Research Initiative on eXotic nuclei).

[1] H. Feshbach, Ann. Phys. (N.Y.) **5**, 357 (1958).
[2] H. Feshbach, Ann. Phys. (N.Y.) **19**, 287 (1962).
[3] E. Tiesinga, A. J. Moerdijk, B. J. Verhaar, and H. T. C. Stoof, Phys. Rev. A **46**, R1167 (1992).
[4] E. Tiesinga, B. J. Verhaar, and H. T. C. Stoof, Phys. Rev. A **47**, 4114 (1993).
[5] A. J. Moerdijk, B. J. Verhaar, and A. Axelsson, Phys. Rev. A **51**, 4852 (1995).
[6] J. R. Taylor, *Scattering Theory: The Quantum Theory on Nonrelativistic Collisions* (Wiley, New York, 1972).
[7] B. Marcelis, E. G. M. van Kempen, B. J. Verhaar, and S. J. J. M. F. Kokkelmans, Phys. Rev. A **70**, 012701 (2004).
[8] N. Nygaard, B. I. Schneider, and P. S. Julienne, Phys. Rev. A **73**, 042705 (2006).
[9] S. J. J. M. F. Kokkelmans, J. N. Milstein, M. L. Chiofalo, R. Walser, and M. J. Holland, Phys. Rev. A **65**, 053617 (2002).
[10] K. Chadan and P. C. Sabatier, *Inverse Problems in Quantum Scattering Theory*, 2nd ed. (Springer, New York, 1989).
[11] J. R. Cox, J. Math. Phys. **5**, 1065 (1964).
[12] R. G. Newton, *Scattering Theory of Waves and Particles*, 2nd ed. (Springer, New York, 1982).
[13] F. Vidal and J. LeTourneux, Phys. Rev. C **45**, 418 (1992).
[14] J.-M. Sparenberg, B. F. Samsonov, F. Foucart, and D. Baye, J. Phys. A **39**, L639 (2006).
[15] B. F. Samsonov, J.-M. Sparenberg, and D. Baye, J. Phys. A **40**, 4225 (2007).
[16] R. D. Amado, F. Cannata, and J.-P. Dedonder, Phys. Rev. A **38**, 3797 (1988).
[17] R. D. Amado, F. Cannata, and J.-P. Dedonder, Phys. Rev. Lett. **61**, 2901 (1988).
[18] A. M. Pupasov, B. F. Samsonov, and J.-M. Sparenberg, e-print arXiv:quant-ph/0709.0343.
[19] H. T. C. Stoof, J. M. V. A. Koelman, and B. J. Verhaar, Phys. Rev. B **38**, 4688 (1988).
[20] J. J. Sakurai, *Modern Quantum Mechanics* (Addison-Wesley, Reading, MA, 1994).
[21] P. J. Leo, C. J. Williams, and P. S. Julienne, Phys. Rev. Lett. **85**, 2721 (2000).
[22] K. M. O'Hara, S. L. Hemmer, S. R. Granade, M. E. Gehm, J. E. Thomas, V. Venturi, E. Tiesinga, and C. J. Williams, Phys. Rev. A **66**, 041401(R) (2002).
[23] E. Arimondo, M. Inguscio, and P. Violino, Rev. Mod. Phys. **49**, 31 (1977).